Article:
Chen, M. orcid.org/0009-0003-3201-9603, Joo, H.-J. orcid.org/0000-0002-4923-9771, Kim, Y. orcid.org/0000-0001-7248-2078 et al. (6 more authors) (2024) Tensile-Strained GeSn Microbridge Lasers with Lithographically Controllable Emission Wavelengths. ACS Photonics. ISSN 2330-4022

https://doi.org/10.1021/acsphotonics.4c01173

Tensile-strained GeSn microbridge lasers with lithographically controllable emission wavelengths

Melvina Chen[1,2†], Hyo-Jun Joo[1†], Youngmin Kim[1], Eng Huat Toh[2], Elgin Quek[2], Zoran Ikonic[3], Wei Du[4,5*], Shui-Qing Yu[4,5*] and Donguk Nam[6*]

[1]School of Electrical and Electronic Engineering, Nanyang Technological University, 50 Nanyang Avenue, Singapore 639798, Singapore

[2]Global Device Engineering, GlobalFoundries Singapore Pte. Ltd, 60 Woodlands Industrial Park D Street 2, Singapore 738406, Singapore

[3]School of Electronic and Electrical Engineering, University of Leeds, Leeds LS2 9JT, UK

[4]Department of Electrical Engineering, University of Arkansas, Fayetteville, Arkansas 72701, USA

[5]Institute for Nanoscience and Engineering, University of Arkansas, Fayetteville, Arkansas 72701, USA

[6]Department of Mechanical Engineering, KAIST, 291 Daehak-ro, Yuseong-gu, Daejeon 34141, Korea

[†]These authors contributed equally to this work.

[*]E-mail: dwnam@kaist.ac.kr; syu@uark.edu; weidu@uark.edu

Abstract

GeSn alloys are considered a promising solution to the long-sought on-chip industry-compatible light sources. Relentless efforts to improve the performance of GeSn lasers include utilizing tensile strain engineering. However, inducing tensile strain in GeSn has been challenging due to residual compressive strain in the GeSn layer, necessitating complex fabrication processes such as multiple deposition of external stressors. Here, we demonstrate tensile-strained GeSn microbridge lasers by harnessing a geometric strain-inversion technique enabled by a single lithography step. Multiple lasers producing different emission wavelengths were fabricated on a single chip by lithographically controlling the amount of tensile strain. Upon the application of tensile strain, the emission wavelength was tuned by more than 45 nm, while the laser threshold was reduced by almost 70%. This work presents a simple cost-effective way to build a large array of on-chip lasers emitting different colors. This method holds a potential for applications such as wavelength division multiplexing with on-chip lasers.

Keywords: *germanium tin, microlasers, group-IV lasers, strain engineering, tunability, silicon photonics*

Introduction

The realization of group IV lasers integrated on a Si platform holds the key to enabling large-scale photonics integration for various crucial applications such as photonics-based quantum computing[1] and artificial neural networks.[2,3] However, due to the fundamental issue of the indirect bandgap nature of group IV elements such as Si and Ge, state-of-the-art on-chip lasers rely extensively on hybrid integration of group III-V lasers.[4,5] While this approach has been effective thus far, the potential of the on-chip III-V lasers may ultimately be limited by various issues including the inherent incompatibility with the existing CMOS fabrication facilities.

Direct bandgap GeSn alloys currently stand as one of the most promising candidates for the realization of fully monolithic lasers on Si since its first demonstration in 2015.[6,7] In recent years, there have been concerted efforts to improve the performance of GeSn lasers toward practical applications such as the realization of room-temperature lasing[8,9] and electrically pumped lasing.[10,11]

Among various strategies for improving the laser performance,[12–20] tensile strain engineering has been considered one of the most effective methods.[21,22] Tensile strain does not only improve the directness of the material but also breaks the degeneracy of valence bands and reduces the density of states, thereby facilitating efficient population inversion that is essential for lasing operation.[23] However, achieving tensile-strained GeSn lasers has been a complex endeavor due to the challenge of intrinsic compressive strain in GeSn. One recent demonstration of tensile-strained GeSn lasers involved the use of multiple external stressor layers throughout the wafer bonding process to induce homogeneous tensile strain distribution on GeSn microdisks.[24] Despite its remarkably low threshold, however, the fabrication process is very complicated, limiting the scalability and CMOS compatibility. Furthermore, the use of external stressor layers deposited on a whole chip prevents the possibility of separately

controlling the amount of tensile strain—and therefore the emission wavelengths—in individual laser devices. The ability to integrate multiple lasers producing emission at different wavelengths on a single chip is valuable for increasing the functionality of integrated photonic chips for various applications such as wavelength-division multiplexing (WDM) optical communications.[25]

In this work, we demonstrate the realization of integrated GeSn lasers with lithographically-defined tensile strains that can produce different emission wavelengths on a single chip. By utilizing a recently demonstrated push-to-pull strain inversion design,[26] we can individually control the amount of tensile strain in many GeSn lasers via a single lithography step. By achieving a tensile strain of up to 0.2% in the GeSn gain medium, we showed the emission wavelength tuning of more than 45 nm, which is also validated by theoretical verification. Our work presents a straightforward and scalable approach to achieve a large-scale array of on-chip GeSn lasers with controllable emission wavelengths, marking a significant step towards fully monolithic and high-functionality photonic-integrated circuits.

Results

Design and fabrication of tensile-strained strain-inversed GeSn microbridge lasers

Figure 1a presents a schematic illustration of strain-inversed GeSn microbridge laser under optical pumping. The laser structure consists of a tensile-strained GeSn microbridge gain medium (illuminated by pump light) surrounded by a pair of corner cube mirrors affixed to two interlocking pads on both sides. The tensile strain along the <100> direction on the gain medium is induced upon undercutting of the Ge sacrificial layer underneath the compressively-strained GeSn. The GeSn interlocked pads are thereupon relaxed, which causes them to expand and push inwards at both sides as indicated by the grey arrows. Consequently, the GeSn microbridge at the center experiences pulling force from opposing pads, resulting in a tensile strain. The GeSn microbridge is optically pumped by a 1550-nm pulsed laser and emission from the microbridge resonates within the cavity formed by two corner cube mirrors before being scattered and collected. Figure 1b shows a scanning electron microscope (SEM) image of a fabricated microbridge. The width and length of the microbridge are 2 μm and 22 μm, respectively. The substrate consists of a $Si_{0.03}GeSn_{0.08}$ (150 nm) cap layer, $GeSn_{0.11}$ (430 nm), and $GeSn_{0.07}$ (670 nm) grown on a Ge buffer (450 nm) on Si wafer. The microbridge consists of the entire (Si)GeSn stack that is above the Ge buffer and has a total thickness of 1.25 μm. The magnitude of optical field distribution by 3D finite-difference time-domain (FDTD) simulation is shown in Figure 1c, demonstrating the excellent light confinement ability in our GeSn cavity design formed by corner cube mirrors.

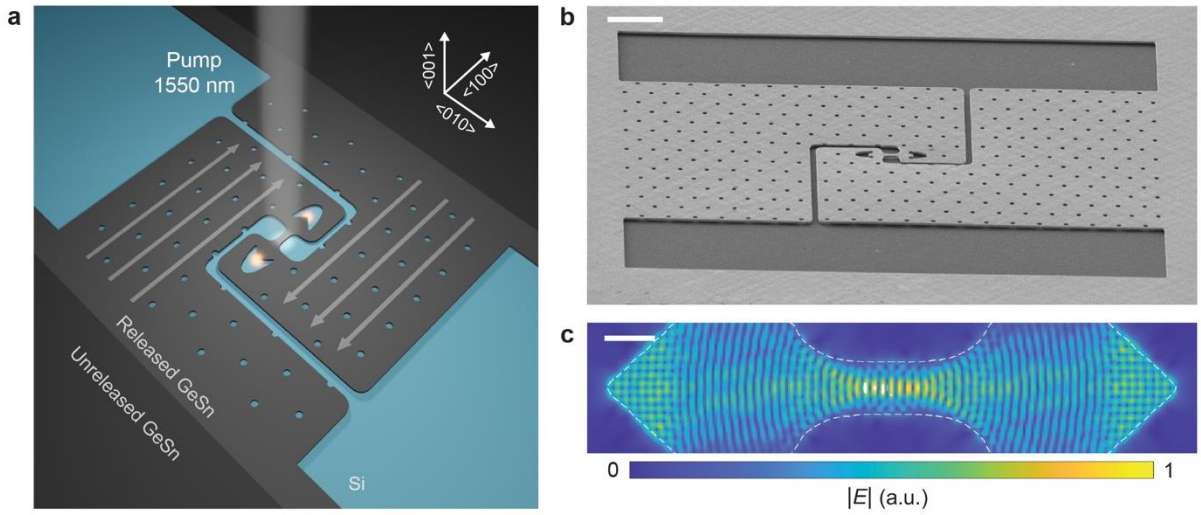

Figure 1. (a) Design and principle of tensile-strained GeSn microbridge laser. GeSn gain medium experiencing tensile strain along <100> direction by the pulling force of opposing pads (grey arrows) is optically pumped by a 1550-nm pulsed laser. Emission is scattered at the corner cube mirrors before being collected. (b) SEM image of a fabricated tensile-strained GeSn microbridge laser. Scale bar, 25 µm. (c) Magnitude of electric field distribution of GeSn cavity with corner cube mirrors simulated by FDTD method. The dashed line represents the microbridge outline. Scale bar, 2 µm.

We performed 3D finite element method (FEM) strain simulation as presented in Figure 2a. The simulated device features a pad length of 245 µm and pad width of 100 µm. Due to vertical Sn variation, there is an in-built strain gradient in the substrate. For the simulation, the initial strain was input as 0.07% for SiGeSn cap, –0.09% for $GeSn_{0.11}$ and –0.08% for the graded $GeSn_{0.07}$ buffer. The numbers were approximated from XRD-RSM data for a similar substrate in reference [27]. Furthermore, the extent of the undercut region is crucial as it directly affects the degree of strain relaxation and, consequently, the strain induced on the microbridge. The undercut region was determined from the experiment and incorporated into the simulation. The simulated profile features a strain gradient across the device. The initial tensile strain of 0.07% in the SiGeSn cap layer inverts to a maximum of ~–0.5% compressive strain, and the initial –0.08% strain in the $GeSn_{0.07}$ buffer inverts to a maximum of ~1% tensile strain. Due to the contrasting strain at the top SiGeSn cap layer and the bottom $GeSn_{0.07}$ buffer layer, the $GeSn_{0.11}$ at the middle of the stack experiences a strain gradient with a maximum tensile strain of 0.2%

near the bottom of the layer. In this study, $GeSn_{0.11}$ with 0.2% strain serves as the gain medium as it has higher directness than GeSn0.07 with ~1% tensile strain.[28]

By keeping the pad length constant at 245 µm and only increasing the pad width, an array of GeSn microbridge lasers of distinctive tensile strain was designed and fabricated. Raman spectroscopy was performed to investigate the tensile strain-induced Raman peak shift of the microbridges after the compressive strain relaxation. A 532-nm laser was focused by ×100 objective lens on the sample which resulted in a spot size of ~1 µm. Power-dependent measurements were conducted to select the appropriate power for measurement and to prevent heating of the sample which may introduce errors in the Raman spectra.[29] Raman spectra of three devices with different pad widths are shown in Figure 2b. Device 1 is expected to be fully relaxed due to a fracture in the pads and is used as the control device. Devices 2 and 3 with pad width of 50 µm and 100 µm have increasing tensile strain which amount to 1.18 cm^{-1} and ~2.24 cm^{-1} Raman blue-shift relative to Device 1, respectively. The Raman spectra are fitted by the Lorentzian function. As there is currently no reliable Raman uniaxial strain-shift coefficient particular to our GeSn substrate in the literature, the strain in the microbridge is determined from the photoluminescence and theoretical calculation results as discussed in the following sections.

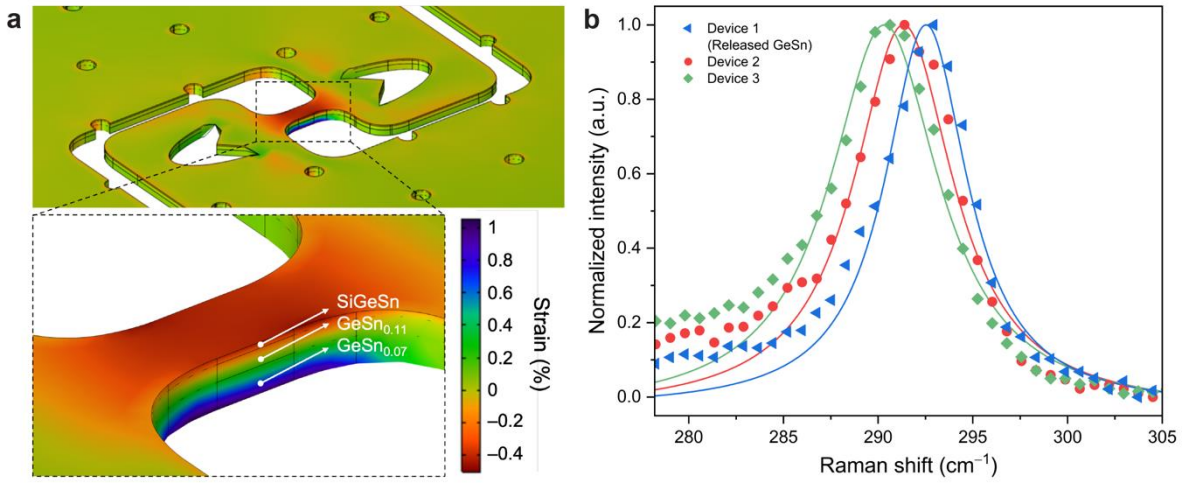

Figure 2. (a) Simulated strain using 3D FEM on a strain-inversed GeSn microbridge cavity with 100-µm pad width. (b) Raman spectra of three devices with varying pad width.

Characterization of GeSn lasers with varying tensile strains

Photoluminescence spectroscopy was conducted to study the emission characteristics of the devices. The chip was mounted in a close-cycle helium cryostat operating at 4 K. A 1550-nm pulsed laser with a repetition rate of 1 MHz and pulse width of 5 ns was focused onto the devices using a ×15 reflective objective lens, resulting in a spot size of ~25 μm. Subsequently, the emitted luminescence from the sample was collected by the same objective lens and guided towards a Fourier-transform infrared (FTIR) spectrometer equipped with an extended InGaAs detector with a cut-off of 2.4 μm.

The normalized emission spectra from the three devices with different strains, confirmed by Raman spectroscopy, are shown in Figure 3a. Three different optical pumping densities for below, near, and above thresholds are presented. At a low pump power density of 6 kW cm^{-2} (first column), all three devices are below their lasing thresholds and only broad spontaneous emissions are observed. At pumping power densities near the thresholds, sharp cavity modes appear on top of the broad spectrum background for all three devices. At 59.7 kW cm^{-2} pump power density (last column), all devices are pumped above their threshold and lasing peaks dominate the background spontaneous emission, providing evidence of lasing. It is worth noting that the peak intensity of Device 3 at 59.7 kW cm^{-2} is 1.2 and 3.2 times higher than those of Devices 2 and 1, respectively. Furthermore, the peak position of Device 3 at 2269.8 nm is redshifted by more than 45 nm compared to Device 1 at 2224.4 nm. The origin of the threshold reduction and the spectral shift will be discussed in Figure 4.

The light-in-light-out (L-L) curves of the devices are plotted in Figure 3b, showing clear threshold behavior. The threshold is extracted as 32.4, 21.4, and 10.2 kW cm^{-2} for Device 1, 2, and 3, respectively. The nearly 70% improvement in the lasing threshold of strained Device 3 relative to unstrained Device 1 is attributed to the increased bandgap directness and favourable valence band splitting by tensile strain[24]. Overall, the benefits of tensile strain on lasing

characteristics are unambiguously presented through the spectral evolution of the lasing peak intensity and position with pumping power density and strain.

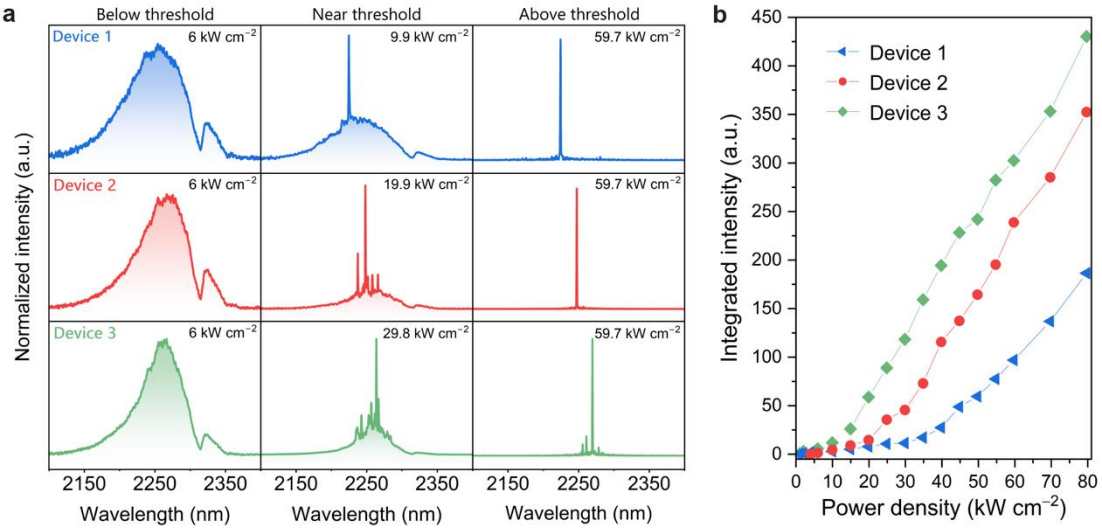

Figure 3. (a) Evolution of emission spectra of devices of varying tensile strain with pumping power densities. (b) Corresponding L-L curves.

Theoretical analysis and simulations

We performed a theoretical gain simulation using the 8-band **k·p** method to understand the photoluminescence behavior and deduce the tensile strain on the microbridges. The calculation was performed for GeSn with 11 at.% Sn at carrier injection of 3×10^{17} cm^{-3} which corresponds to ~59.7 kW cm^{-2} pumping power. Figure 4a shows the optical net gain spectra for three uniaxial tensile strain values: 0%, 0.1%, and 0.2%. The gain peak intensity increases and redshifts with increasing tensile strain.

The lasing emission of control Device 1 at ~2224.4 nm coincides with the 0% strain relaxed gain profile peak. Meanwhile, for Device 2, the emission peak wavelength is shifted by ~23 nm relative to Device 1 to 2247.4 nm. The ~23 nm shift is in reasonably good agreement with the free spectral range (FSR) of the cavity calculated from the equation $\Delta\lambda = \frac{\lambda^2}{2nL}$, where n is refractive index and L is cavity length. Furthermore, the lasing peak of Device 2 largely aligns with 0.1% gain profile peak, therefore the strain in Device 2 is deduced to be 0.1%.

Hence, we attribute the observed shift to the cavity mode-hopping induced by the gain spectrum shift. For Device 3, the emission peak appears at 2269.8 nm, redshifted by ~45 nm, and two FSRs away relative to unstrained Device 1. The lasing peak coincides with the gain peak of 0.2%, thus we can qualitatively infer that the strain on the device is 0.2%. This result is in good agreement with the tensile strain deduced from 3D FEM simulation in Figure 2a. More precise strain measurement can be possible by harnessing X-ray microdiffraction,[30] which is the subject of further research.

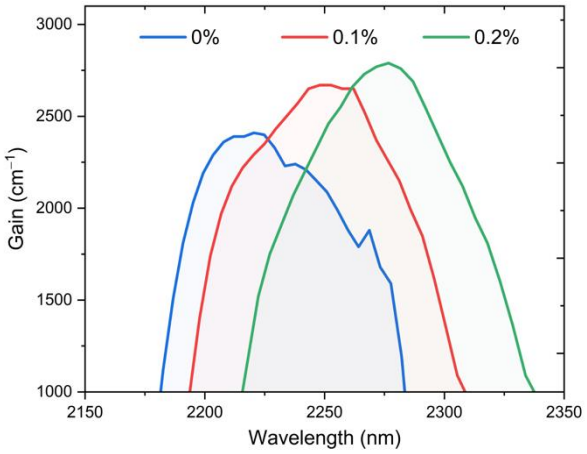

Figure 4. Calculated gain spectra of three values of uniaxial tensile strain at 4 K.

Conclusion

In summary, we have demonstrated a novel technique to achieve tensile-strained GeSn lasers with lithographically controllable emission wavelengths fabricated from compressively strained GeSn layers. By manipulating the tensile strain via geometrical variations, we tuned the emission wavelength by more than 45 nm and achieved improved lasing thresholds. Compared to previous complex approaches involving external stressors[24] or pre-strained GeSn layers,[31] our method stands out for its simplicity and versatility. For practical applications, higher Sn content substrates and the accompanying in-built compressive strain could be beneficial for achieving high tensile strain through strain-inversion technique, potentially enabling low-threshold lasing at room temperature. Additionally, the geometry of our device can be further optimized to enhance the strain inversion factor, such as by decreasing microbridge length and narrowing microbridge width. While additional research is necessary to fully realize the scalability and integration of this approach, our platform presents a promising pathway for practical large-scale integrated photonics.

Author contributions

M.C. and H.-J.J. contributed equally to this work.

Competing financial interests

The authors declare no competing financial interests.

Acknowledgements

The authors would like to acknowledge and thank the Nanyang NanoFabrication Centre (N2FC).

Funding Sources

National Research Foundation (NRF), Singapore-A*STAR Joint Grant (Quantum Engineering Programme (NRF2022-QEP2-02-P13)).

References

(1) Pelucchi, E.; Fagas, G.; Aharonovich, I.; Englund, D.; Figueroa, E.; Gong, Q.; Hannes, H.; Liu, J.; Lu, C. Y.; Matsuda, N.; Pan, J. W.; Schreck, F.; Sciarrino, F.; Silberhorn, C.; Wang, J.; Jöns, K. D. The Potential and Global Outlook of Integrated Photonics for Quantum Technologies. *Nat. Rev. Phy*. **2022**, 194–208.

(2) Bogaerts, W.; Pérez, D.; Capmany, J.; Miller, D. A. B.; Poon, J.; Englund, D.; Morichetti, F.; Melloni, A. Programmable Photonic Circuits. *Nature* **2020**, 207–216.

(3) Shastri, B. J.; Tait, A. N.; Ferreira de Lima, T.; Pernice, W. H. P.; Bhaskaran, H.; Wright, C. D.; Prucnal, P. R. Photonics for Artificial Intelligence and Neuromorphic Computing. *Nat. Photonics* **2021**, 102–114.

(4) Xiang, C.; Jin, W.; Terra, O.; Dong, B.; Wang, H.; Wu, L.; Guo, J.; Morin, T. J.; Hughes, E.; Peters, J.; Ji, Q.-X.; Feshali, A.; Paniccia, M.; Vahala, K. J.; Bowers, J. E. 3D Integration Enables Ultralow-Noise Isolator-Free Lasers in Silicon Photonics. *Nature* **2023**, *620* (7972), 78–85.

(5) Lihachev, G.; Riemensberger, J.; Weng, W.; Liu, J.; Tian, H.; Siddharth, A.; Snigirev, V.; Shadymov, V.; Voloshin, A.; Wang, R. N.; He, J.; Bhave, S. A.; Kippenberg, T. J. Low-Noise Frequency-Agile Photonic Integrated Lasers for Coherent Ranging. *Nat Commun.* **2022**, *13* (1).

(6) Wirths, S.; Geiger, R.; Von Den Driesch, N.; Mussler, G.; Stoica, T.; Mantl, S.; Ikonic, Z.; Luysberg, M.; Chiussi, S.; Hartmann, J. M.; Sigg, H.; Faist, J.; Buca, D.; Grützmacher, D. Lasing in Direct-Bandgap GeSn Alloy Grown on Si. *Nat. Photonics* **2015**, *9* (2), 88–92.

(7) Homewood, K. P.; Lourenço, M. A. The Rise of the GeSn Laser. *Nat. Photonics* **2015**, *9* (2), 78–79.

(8) Chrétien, J.; Thai, Q. M.; Frauenrath, M.; Casiez, L.; Chelnokov, A.; Reboud, V.; Hartmann, J. M.; El Kurdi, M.; Pauc, N.; Calvo, V. Room Temperature Optically Pumped GeSn Microdisk Lasers. *Appl. Phys. Lett.* **2022**, *120* (5).

(9) Buca, D.; Bjelajac, A.; Spirito, D.; Concepción, O.; Gromovyi, M.; Sakat, E.; Lafosse, X.; Ferlazzo, L.; von den Driesch, N.; Ikonic, Z.; Grützmacher, D.; Capellini, G.; El Kurdi, M. Room Temperature Lasing in GeSn Microdisks Enabled by Strain Engineering. *Adv. Opt. Mater.* **2022,** 10, 2201024.

(10) Zhou, Y.; Ojo, S.; Wu, C.-W.; Miao, Y.; Tran, H.; Grant, J. M.; Abernathy, G.; Amoah, S.; Bass, J.; Salamo, G.; Du, W.; Chang, G.-E.; Liu, J.; Margetis, J.; Tolle, J.; Zhang, Y.-H.; Sun, G.; Soref, R. A.; Li, B.; Yu, S.-Q. Electrically Injected GeSn Lasers with Peak Wavelength up to 2.7 μm. *Photonics Res.* **2022**, *10* (1), 222.

(11) Zhou, Y.; Miao, Y.; Ojo, S.; Tran, H.; Abernathy, G.; Grant, J. M.; Amoah, S.; Salamo, G.; Du, W.; Liu, J.; Margetis, J.; Tolle, J.; Zhang, Y.; Sun, G.; Soref, R. A.; Li, B.; Yu, S.-Q. Electrically Injected GeSn Lasers on Si Operating up to 100 K. *Optica* **2020**, *7* (8), 924–928.

(12) von den Driesch, N.; Stange, D.; Rainko, D.; Povstugar, I.; Zaumseil, P.; Capellini, G.; Schröder, T.; Denneulin, T.; Ikonic, Z.; Hartmann, J. M.; Sigg, H.; Mantl, S.; Grützmacher, D.; Buca, D. Advanced GeSn/SiGeSn Group IV Heterostructure Lasers. *Advanced Science* **2018**, *5* (6).

(13) Elbaz, A.; Arefin, R.; Sakat, E.; Wang, B.; Herth, E.; Patriarche, G.; Foti, A.; Ossikovski, R.; Sauvage, S.; Checoury, X.; Pantzas, K.; Sagnes, I.; Chrétien, J.; Casiez, L.; Bertrand, M.; Calvo, V.; Pauc, N.; Chelnokov, A.; Boucaud, P.; Boeuf, F.; Reboud, V.; Hartmann, J. M.; El Kurdi, M. Reduced Lasing Thresholds in GeSn Microdisk Cavities with Defect Management of the Optically Active Region. *ACS Photonics* **2020**, *7* (10), 2713–2722.

(14) Jung, Y.; Burt, D.; Zhang, L.; Kim, Y.; Joo, H.-J.; Chen, M.; Assali, S.; Moutanabbir, O.; Seng Tan, C.; Nam, D. Optically Pumped Low-Threshold Microdisk Lasers on a GeSn-on-Insulator Substrate with Reduced Defect Density. *Photonics Res.* **2022**, *10* (6), 1332.
(15) Kim, Y.; Assali, S.; Burt, D.; Jung, Y.; Joo, H. J.; Chen, M.; Ikonic, Z.; Moutanabbir, O.; Nam, D. Enhanced GeSn Microdisk Lasers Directly Released on Si. *Adv. Opt. Mater.* **2022**, *10* (2).
(16) Stange, D.; Von Den Driesch, N.; Zabel, T.; Armand-Pilon, F.; Rainko, D.; Marzban, B.; Zaumseil, P.; Hartmann, J. M.; Ikonic, Z.; Capellini, G.; Mantl, S.; Sigg, H.; Witzens, J.; Grützmacher, D.; Buca, D. GeSn/SiGeSn Heterostructure and Multi Quantum Well Lasers. *ACS Photonics* **2018**, *5* (11), 4628–4636.
(17) Sun, G.; Soref, R. A.; Cheng, H. H. Design of an Electrically Pumped SiGeSn/GeSn/SiGeSn Double-Heterostructure Midinfrared Laser. *J. Appl. Phys.* **2010**, *108* (3).
(18) Kim, Y.; Joo, H. J.; Chen, M.; Son, B.; Burt, D.; Shi, X.; Zhang, L.; Ikonic, Z.; Tan, C. S.; Nam, D. High-Precision Wavelength Tuning of GeSn Nanobeam Lasers via Dynamically Controlled Strain Engineering. *Advanced Science* **2023**, *10* (17).
(19) Joo, H. J.; Kim, Y.; Chen, M.; Burt, D.; Zhang, L.; Son, B.; Luo, M.; Ikonic, Z.; Lee, C.; Cho, Y. H.; Tan, C. S.; Nam, D. All-Around HfO2 Stressor for Tensile Strain in GeSn-on-Insulator Nanobeam Lasers. *Adv. Opt. Mater.* **2023,** 11, 2301115.
(20) Burt, D.; Zhang, L.; Jung, Y.; Joo, H.-J.; Kim, Y.; Chen, M.; Son, B.; Fan, W.; Ikonic, Z.; Tan, C. S.; Nam, D. Tensile Strained Direct Bandgap GeSn Microbridges Enabled in GeSn-on-Insulator Substrates with Residual Tensile Strain. *Opt. Lett.* **2023**, *48* (3), 735.
(21) Sukhdeo, D.; Kim, Y.; Gupta, S.; Saraswat, K.; Dutt, B.; Nam, D. Theoretical Modeling for the Interaction of Tin Alloying with N-Type Doping and Tensile Strain for GeSn Lasers. *IEEE Electron Device Letters* **2016**, *37* (10), 1307–1310.
(22) Nam, D.; Sukhdeo, D. S.; Gupta, S.; Kang, J. H.; Brongersma, M. L.; Saraswat, K. C. Study of Carrier Statistics in Uniaxially Strained Ge for a Low-Threshold Ge Laser. *IEEE J. on Selected Topics in Quantum Electronics* **2014**, *20* (4).
(23) Sukhdeo, D. S.; Kim, Y.; Gupta, S.; Saraswat, K. C.; Dutt, B. R.; Nam, D. Anomalous Threshold Reduction from <100> Uniaxial Strain for a Low-Threshold Ge Laser. *Opt Commun* **2016**, *379*, 32–35.
(24) Elbaz, A.; Buca, D.; von den Driesch, N.; Pantzas, K.; Patriarche, G.; Zerounian, N.; Herth, E.; Checoury, X.; Sauvage, S.; Sagnes, I.; Foti, A.; Ossikovski, R.; Hartmann, J. M.; Boeuf, F.; Ikonic, Z.; Boucaud, P.; Grützmacher, D.; El Kurdi, M. Ultra-Low-Threshold Continuous-Wave and Pulsed Lasing in Tensile-Strained GeSn Alloys. *Nat Photonics* **2020**, *14* (6), 375–382.
(25) Dong, P. Silicon Photonic Integrated Circuits for Wavelength-Division Multiplexing Applications. *IEEE J. of Selected Topics in Quantum Electronics* **2016**, *22* (6), 370–378.
(26) Burt, D.; Joo, H. J.; Kim, Y.; Jung, Y.; Chen, M.; Luo, M.; Kang, D. H.; Assali, S.; Zhang, L.; Son, B.; Fan, W.; Moutanabbir, O.; Ikonic, Z.; Tan, C. S.; Huang, Y. C.; Nam, D. Direct Bandgap GeSn Nanowires Enabled with Ultrahigh Tension from Harnessing Intrinsic Compressive Strain. *Appl. Phys. Lett.* **2022**, *120* (20).
(27) Acharya, S.; Stanchu, H.; Kumar, K.; Ojo, S.; Benamara, M.; Chang, G.E.; Li, B.; Du, Wei.; and Yu, S. Q. Electrically Injected Mid-Infrared GeSn Laser on Si Operating at 140 K. arXiv:2405.10163v1.

(28) Reboud, V.; Buca, D.; Sigg, H.; Hartmann, J. M.; Ikonic, Z.; Pauc, N.; Calvo, V.; Rodriguez, P.; Chelnokov, A. Silicon Photonics IV: Innovative Frontiers. *Springer Link*, 2021.
(29) Joo, H. J.; Kim, Y.; Burt, D.; Jung, Y.; Zhang, L.; Chen, M.; Parluhutan, S. J.; Kang, D. H.; Lee, C.; Assali, S.; Ikonic, Z.; Moutanabbir, O.; Cho, Y. H.; Tan, C. S.; Nam, D. 1D Photonic Crystal Direct Bandgap GeSn-on-Insulator Laser. *Appl. Phys. Lett.* **2021**, *119* (20).
(30) Gassenq, A.; Tardif, S.; Guilloy, K.; Osvaldo Dias, G.; Pauc, N.; Duchemin, I.; Rouchon, D.; Hartmann, J. M.; Widiez, J.; Escalante, J.; Niquet, Y. M.; Geiger, R.; Zabel, T.; Sigg, H.; Faist, J.; Chelnokov, A.; Rieutord, F.; Reboud, V.; Calvo, V. Accurate Strain Measurements in Highly Strained Ge Microbridges. *Appl. Phys. Lett.* **2016**, *108* (24).
(31) Chrétien, J.; Pauc, N.; Armand Pilon, F.; Bertrand, M.; Thai, Q. M.; Casiez, L.; Bernier, N.; Dansas, H.; Gergaud, P.; Delamadeleine, E.; Khazaka, R.; Sigg, H.; Faist, J.; Chelnokov, A.; Reboud, V.; Hartmann, J. M.; Calvo, V. GeSn Lasers Covering a Wide Wavelength Range Thanks to Uniaxial Tensile Strain. *ACS Photonics* **2019**, *6* (10), 2462–2469.

For Table of Contents Use Only

Tensile-strained GeSn microbridge lasers with lithographically controllable emission wavelengths

Melvina Chen, Hyo-Jun Joo, Youngmin Kim, Eng Huat Toh, Elgin Quek, Zoran Ikonic, Wei Du, Shui-Qing Yu and Donguk Nam

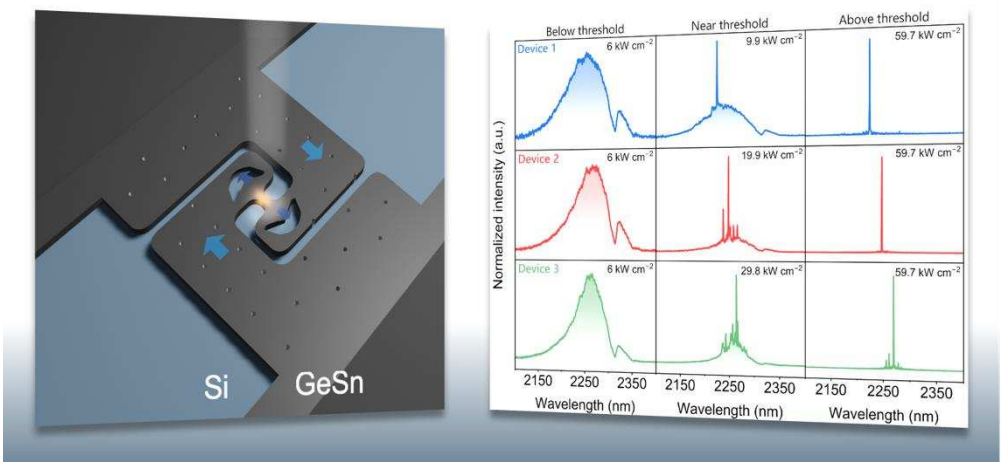

Synopsis:

(Left) Strain-inversed GeSn microbridge laser. (Right) Emission of different laser devices.